Matter

Article

Amphiphilic deformable interconnects for stretchable thermoelectrics

Graphical abstract

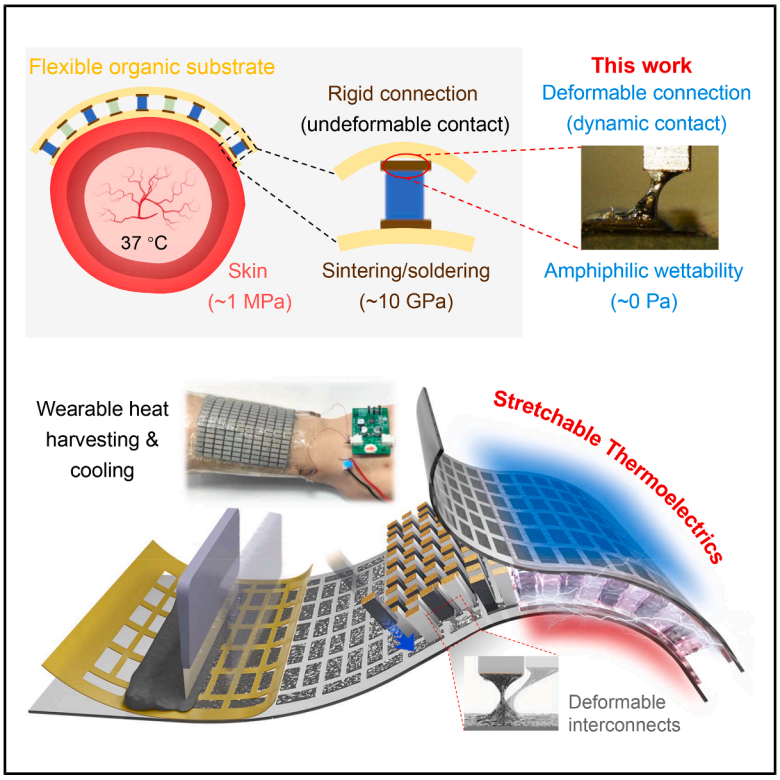

Highlights

- 120% multi-axial deformation between substrates and TE legs with OEC interconnects
- Soft welding and alignment of TE legs for integration through mutual wetting structure
- Device-level 83% stretchability alongside a normalized power density of 1.178 μW cm^{-2} K^{-2}

Authors

Zhangli Du, Yi Zhou, Shuwen Chen, ..., Ghim Wei Ho, Jiaqing He, Tianpeng Ding

Correspondence

wk_xie@uestc.edu.cn (W.X.), elehgw@nus.edu.sg (G.W.H.), hejq@sustech.edu.cn (J.H.), dingtp@uestc.edu.cn (T.D.)

In brief

We developed a deformable electrode that acts like a "liquid solder," enabling robust and stable connections between rigid thermoelectric materials and soft substrates. Wearable devices fabricated with this technology combine excellent stretchability with high power generation efficiency, capable of driving a pedometer using only body heat and providing active skin cooling without heat sink.

Demonstrate
Proof-of-concept of performance with intended application/response

Du et al., 2026, Matter 9, 102653
April 1, 2026
https://doi.org/10.1016/j.matt.2026.102653

CellPress

Matter

CellPress

Article

Amphiphilic deformable interconnects for stretchable thermoelectrics

Zhangli Du,[1,7] Yi Zhou,[2,3,7,8] Shuwen Chen,[4,7] Wenke Xie,[1,*] Sitong Li,[1] Xinyu Chen,[1] Yongqi Tan,[1] Xu Xiao,[1] Ghim Wei Ho,[3,5,*] Jiaqing He,[2,6,*] and Tianpeng Ding[1,9,*]

[1]School of Physics, State Key Laboratory of Electronic Thin Film and Integrated Devices, University of Electronic Science and Technology of China, Chengdu, Sichuan 611731, China

[2]Department of Physics, State Key Laboratory of Quantum Functional Materials, and Guangdong Basic Research Center of Excellence for Quantum Science, Southern University of Science and Technology, Shenzhen 518055, China

[3]Department of Electrical and Computer Engineering, and Advanced Research and Technology Innovation Center (ARTIC), National University of Singapore, Singapore 117581, Singapore

[4]Institute of Medical Equipment Science and Engineering, Huazhong University of Science and Technology, Wuhan 430074, China

[5]Department of Materials Science and Engineering, National University of Singapore, Singapore 117575, Singapore

[6]Guangdong Provincial Key Laboratory of Advanced Thermoelectric Materials and Device Physics, and Shenzhen Key Laboratory of Thermoelectric Materials, Southern University of Science and Technology, Shenzhen 518055, China

[7]These authors contributed equally

[8]Present Address: School of Electronic Science and Engineering, Southeast University, Nanjing 210096, China

[9]Lead contact

*Correspondence: wk_xie@uestc.edu.cn (W.X.), elehgw@nus.edu.sg (G.W.H.), hejq@sustech.edu.cn (J.H.), dingtp@uestc.edu.cn (T.D.)

https://doi.org/10.1016/j.matt.2026.102653

PROGRESS AND POTENTIAL Wearable thermoelectric (TE) devices hold great potential for sustainable power generation in body-worn electronics by harvesting body heat. While significant advances have been made in TE materials, critical challenges remain in achieving reliable device integration that accommodates skin deformation without compromising performance or durability. Conventional rigid interconnects based on tin soldering are prone to mechanical stress and electrical instability due to modulus mismatch with flexible substrates, which significantly hinders their practical applicability. Here, we present a paradigm-shift strategy using amphiphilic organic-eutectic composite (OEC) interconnects to address this fundamental incompatibility. The interconnects decorated with macromolecules achieve adaptive affinity with both TE legs and organic substrates, thereby significantly enhancing electromechanical contact and structural robustness. This strategy enables scalable manufacturing of flexible TE modules with high integration capability (160 pairs) through printable processing, while also achieving device-level stretchability of ~80% alongside a negligible resistance change of <5% after 20,000 bending cycles. Together with the low electrical contact resistance of OEC interconnects and large thermal resistance of air gap between TE legs, our on-body wearable TE device can sustain a commercial pedometer and realize active skin temperature cooling. This work provides a new solution not only for stretchable TE devices with robust heterointerconnects but also for the heterogeneous integration of emerging wearable electronics.

SUMMARY

On-body heat harvesting with thermoelectric (TE) devices promises sustainable power supply for wearable electronics and body sensor networks. Conventional wearable TEs use soldered rigid-flex interfaces to conform to skin morphology, where the modulus mismatch between TE legs and the substrate brings forth an unstable electromechanical connection. Here, we develop a paradigm-shift strategy to advance wearable TE devices with amphiphilic deformable interconnects. Particularly, the amphiphilic organic-eutectic composite (OEC) decorated with macromolecules achieves adaptive affinity with both TE legs and organic substrates, improving electromechanical contact and robustness substantially. Also, the printable and adhesive OEC simplifies the device manufacturing process with scalability and integration capability of up to 160 pairs of TE legs. As a result, a proof-of-concept device exhibits prototype-level stretchability of ~80% and electromechanical stability with <5% resistance change even after 20,000 bending cycles. This work provides

a solution for both stretchable devices with robust heterointerconnects and heterogeneous integration of wearable electronics.

INTRODUCTION

The ever-increasing demands of personalized and wearable healthcare (such as physical vital monitoring,[1,2] rehabilitation therapy,[3–5] and artificial electronic skin[6–8]) necessitate a self-sustained and robust power supply for unremitting body area networking and communication. Thermoelectric (TE) devices can not only harvest waste body heat for electricity generation but also be used for personalized cooling, which is scarce yet increasingly important in healthcare.[9–11] However, the power output and wearable comfort of TE devices are determined by the components, including TE materials, electrodes, and substrates.[12] Traditionally, inorganic rigid TE materials are soldered with fragile/brittle ceramic substrates (Figure S1A), which makes it difficult to meet the requirements of wearable electronic devices such as lightweight, stretchable, and robust.[13,14] Moreover, because of the irregular shape and dynamic deformation of skin, the rigid solder layer between inorganic TE materials and electrodes is unconformable and less efficient for harvesting heat from the skin,[15] which is detrimental to heat harvesting or temperature management of wearables.

To date, many strategies have been developed to improve the flexibility and compatibility of TE devices, of which one attempt involves utilizing organic TEs with intrinsically flexible features. However, organic TEs suffer from low electrical properties, and thus, the average figure of merit (zT) is less than 1.0 for tiny thermal gradient harvesting at room temperature.[16–19] Another more widely used and practical approach is to sandwich rigid inorganic TE legs/films between two flexible organic substrates (polyimide or polydimethylsiloxane) via tin soldering (Figure S1B).[20–23] Nonetheless, the common rigid tin soldering between inorganic TE legs and organic substrate is prone to failure in electrothermal connection when subjected to repeated deformation, due to the stress concentration rising from the huge difference of intrinsic Young's moduli between TE legs and substrates.[24,25] Consequently, advanced contact technologies that can provide a deformable interconnection at the inorganic-organic heterointerface with good flexibility and electromechanical robustness are urged to be developed, which is also pivotal to ensure conformal contact with dynamic complex geometries of the human body for optimal TE performance.[26,27]

Gallium (Ga)-based liquid metal (LM) alloys offer a compelling platform for developing deformable interconnects in stretchable TE generators. Owing to their intrinsic fluidity, high electrical conductivity, and extreme stretchability,[28,29] LMs in various forms (e.g., pure melts,[30–32] alloy composites,[33–35] and LM particle-elastomer mixtures[36,37]) have been explored as deformable interconnects in thermoelectric generators (TEGs).[16,23,38,39] Typically, eGaIn is confined within microchannels embedded in polydimethylsiloxane (PDMS) substrates to form electrical connections between n- and p-type TE elements.[23,40] However, the complex fabrication process and high surface tension of LMs often lead to issues in patterning stability and mechanical reliability under deformation, thereby constraining the achievable integration density and scalability of such devices. Further progress has been made with LM-embedded elastomers, which exhibit favorable electrical and thermal properties and have been widely adopted. For instance, one study demonstrated the integration of 100 TE legs using LM-embedded elastomers, achieving a power density of 86.6 $\mu W\ cm^{-2}$ under a temperature difference of 60°C. Nevertheless, the fundamental mechanical mismatch at the soft-hard interface between the TE legs and the polymer matrix remains inadequately addressed. This often necessitates the use of additional PDMS molds for leg alignment, which not only complicates fabrication but also introduces parasitic thermal pathways that ultimately limit the power output of the device.[39]

Herein, we report a deformable interconnect strategy based on amphiphilic organic-eutectic composite (OEC) for the fabrication of stretchable and robust on-body TE devices. Through a stencil printing and self-assemble process, the eutectic gallium-indium (eGaIn) and organic macromolecular in the OEC are redistributed accordingly to achieve amphiphilicity with both organic substrates and inorganic TE legs. The amphiphilicity and fluidic nature of the OEC form a soft electrical interconnection between the substrate and TE legs, capable of multi-axial bending with displacement resilience while maintaining stable electromechanical contact (e.g., up to 150% of the dimension of TE legs with a resistance variation of <1%). In addition, the adequate adhesiveness of OEC through stencil printing is conducive to the fixation of TE legs, which greatly simplifies the device fabrication process with scalability and integration capability. Consequently, our TE device, composed of 160 pairs of Bi_2Te_3/Sb_2Te_3 legs, possesses prototype-level stretchability of up to 80% and electromechanical stability with negligible resistance change of <5% after 20,000 bending cycles. Moreover, the as-developed TE device achieves an on-body temperature drop of ~2°C and powers a commercial pedometer continuously when worn on the arm.

RESULTS AND DISCUSSION

The fabrication process of stretchable TE devices with amphiphilic deformable interconnects is schematically illustrated in Figure 1. In particular, the device is constituted by stretchable thermoplastic polyurethane (TPU) substrates, OEC electrodes, and p- and n-type TE legs (see methods). The mutual wetting structure can be formed between the TPU substrate and inorganic TE legs, endowing a relative deformation of heterointerfaces in both horizontal and vertical directions while maintaining robust electrical interconnection (inset in Figures 1A and S2). Moreover, the bonding force between the substrate and TE legs is large enough to adhere the TE legs upside-down or side-hung (Figure S3). Therefore, the TE legs can maintain a stable electromechanical connection despite the position deviation under externally applied stress. It is worth noting that, due to the surface wettability of polyurethane (PU)

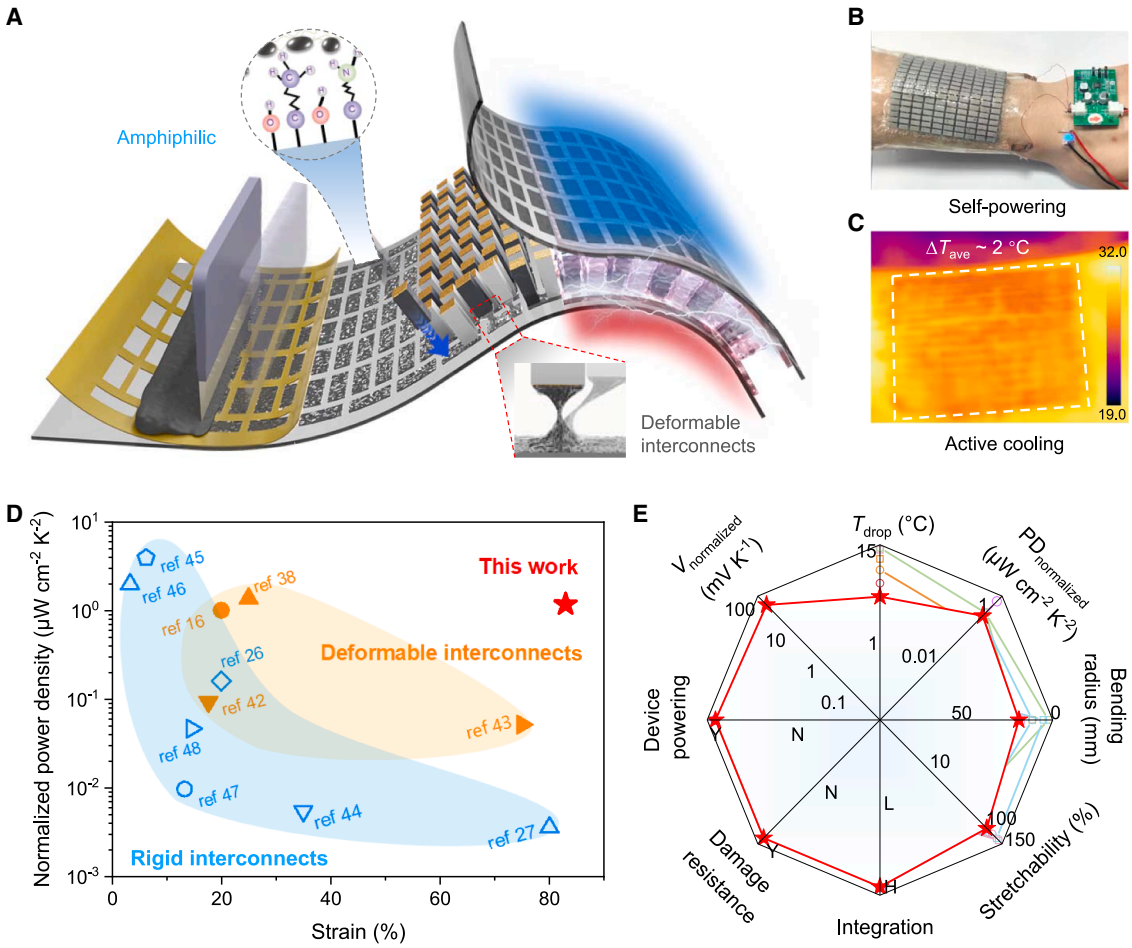

Figure 1. Configuration and state-of-the-art performance of the stretchable TE device based on deformable interconnects

(A) Schematic fabrication process of the flexible TE device.

(B) Photo of on-body self-sustained LED indicator via the flexible TE device.

(C) Infrared image of on-body cooling via the flexible TE device.

(D) Benchmarked normalized power density and stretchability of bulk leg-based TE devices with rigid interconnects (light red shaded area), soft interconnects (light blue shaded area), and our as-fabricated TE device. Detailed comparison can be found in Table S1.

(E) Radar plot with multi-dimensional parameter comparisons between as-fabricated TE device and others reported in the literature. Detailed comparisons can be found in Table S2.

solution and the subsequent evaporation of solvent, PU only forms a thin but dense packaging layer on the surface of the TE legs while maintaining a large amount of air between n- and p-type TE legs (Figure S4). Such confined/enlarged air gap facilitates heat flux matching between the human skin and TE legs,[15,21] and thus, a higher power density can be generated. Notably, the as-fabricated TE device possesses superior flexibility, stretchability, and TE performance, which can power commercial electronics exclusively relying on human body temperature (Figure 1B). Moreover, the TE device also demonstrates on-body cooling ability when worn on the arm (Figure 1C). Compared to other inorganic leg-based TE devices with rigid interconnects (e.g., tin soldering) or soft interconnects (e.g., LM soldering), our device combines the merits of high normalized power density and stretchability (Figure 1D; Table S1) owing to deformable OEC.[16,27,38,41–48] The comparison of state-of-the-art properties between this device and other TE wearables in eight aspects, including temperature drop, normalized power density, flexibility, stretchability, integration level, damage resistance, device powering, and normalized generated voltage, is summarized as well (Figure 1E; Note S1; Table S2).[10,13,16,26,27,38,42,44,45,49–55] Our work (marked as red pentagram) outperforms other flexible TEs, including bulk, film and fiber types, in most aspects, demonstrating remarkable overall properties.

Amphipathicity and contact characterization of OEC interconnects

The OEC ink was formed by dispersing eGaIn particles in cyclohexanone through sonicating and then mixed with a polyester polyol-rich thermoplastic polyurethane binder to form a suspension compound. After circuit activation, the compound was

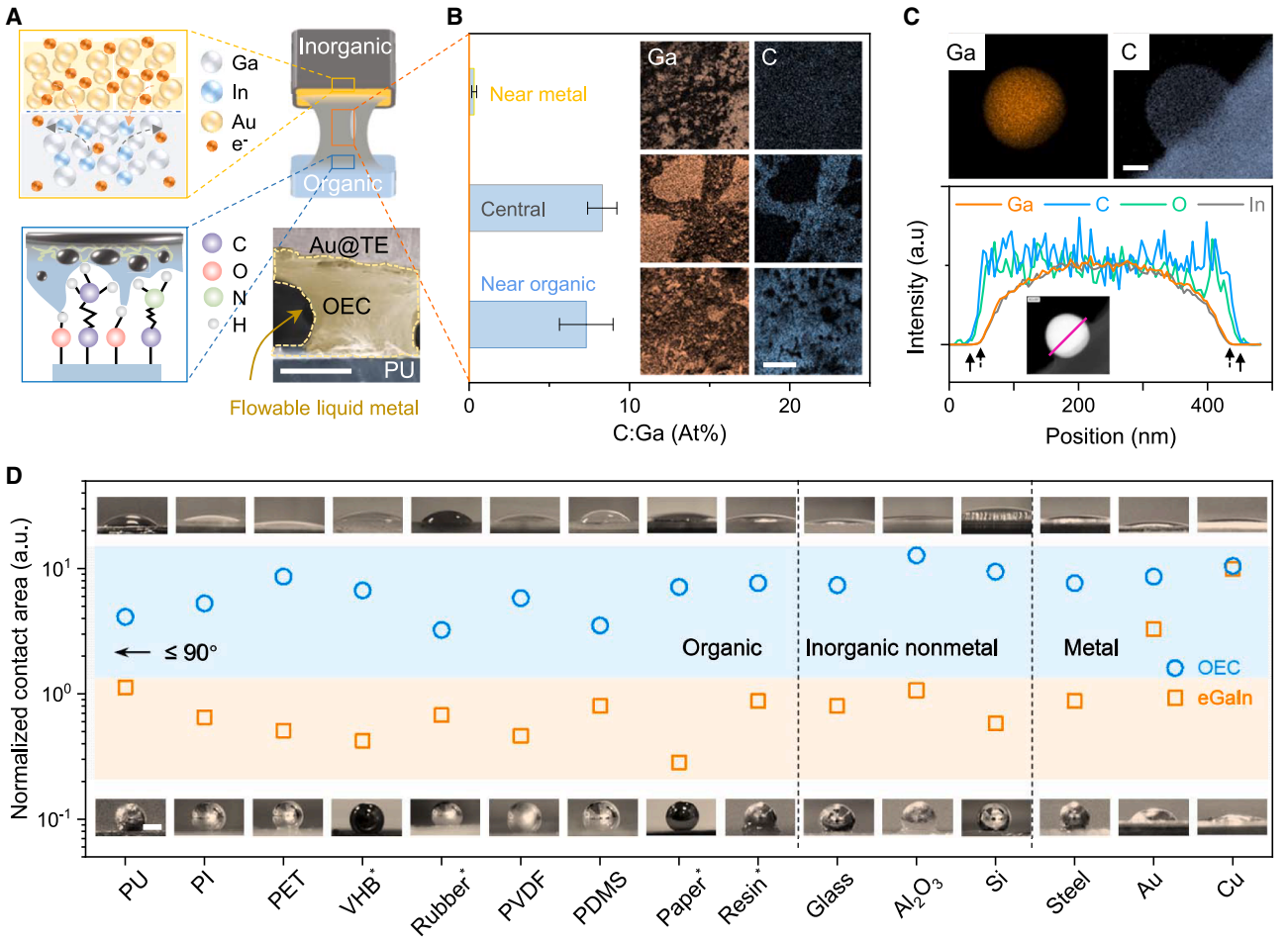

Figure 2. Amphipathicity and contact characterization of OEC interconnects

(A) Schematic illustration (left) and SEM image (bottom right) of OEC interconnects between the TE leg and PU substrate showing the amphipathic property; deformable eGaIn is concentrated in the region marked with yellow pseudo-color. Scale bars: 150 μm.

(B) SEM-EDS mapping and atom ratio of carbon: gallium at different local positions across OEC interfaces, including near metal, central, and near organic substrate, showing the heterogeneous distribution of elements in OEC interconnects. Scale bars: 20 μm.

(C) TEM-EDS mapping of gallium and carbon elements of the eGaIn particles in OEC ink. The line scan reveals the carbon and oxygen increasing above baseline at the particle edge prior to the gallium and indium. Scale bars: 100 nm.

(D) Normalized contact area of eGaIn and OEC ink on various substrates, including organic (polyurethane [PU], polyimide [PI], polyethylene terephthalate [PET], 3M Scotch 4910 VHB [VHB*], silicone rubber (methyl vinyl silicone rubber) [Rubber*], polyvinylidene fluoride [PVDF], polydimethylsiloxane [PDMS], Deli A4 printer paper [Paper*], and epoxy resin [Resin]), inorganic nonmetal (glass, Al_2O_3, and Si), and metal (steel, Au, and Cu) materials. The blue and red shadows are separated by a contact angle of 90°. Scale bars: 1 mm.

redistributed to form a continuous LM layer externally while sustaining a composite layer with LM particles internally (see methods and Figures S5 and S6). Under applied shear stress, larger eGaIn particles or those far from the substrate rupture preferentially, releasing LM that coalesces into a conductive surface network. Smaller or substrate-proximal particles remain mostly intact, contributing to interfacial retention. This spatially differentiated activation yields an amphiphilic structure: the fluid LM top layer ensures high conductivity, while the polymer-rich bottom layer, aided by hydroxyl-functionalized eGaIn particles, bonds strongly with the substrate. As a result, the OEC electrode achieved mutual wetting with both organic substrates and inorganic TE legs (Figure 2A) and can be stretched into a hyperbolic amphiphilic structure owing to high fluidity and stickiness.[56] Through the contact between the LM layer and the Au layer via shear stress, forming $AuGa_2$ to improve wettability, the LM layer enables the wetting of the Au-coated side of TE legs while maintaining non-wetting at other bare surfaces (Figure S7). For the organic substrates, the abundant polar groups of the TPU ensure a strong affinity between the OEC ink and the TPU substrate.[56] These results were validated further using scanning electron microscopy (SEM) and energy dispersive spectroscopy (EDS) mapping (Figures 2B and S8), which revealed composition distribution in the mutual wetting structure. In particular, on the gold layer side, as the Ga atoms chemically infiltrate the gold layer while the organic macromolecular cannot form a stable

connection with the metal, the ratio of carbon to Ga dropped significantly compared to the central body region of the OEC electrode. On the organic substrate side, by contrast, it can be observed that after multiple stripping processes, the ratio of eGaIn elements remains consistent with that of central region, indicating that the ink forms a robust bond with the organic substrate owing to its abundant polar groups.

To explore the nanoscale connection of TPU to LM particles, transmission electron microscopy (TEM) was used to characterize LM particles in OEC ink (Figures 2C and S9), where EDS mappings showed the element distribution of the four typical Ga (Ga), indium (In), oxygen (O), and carbon (C) signals. In the composite, carbon element is attributed to TPU, while Ga and In are the composition of LM layer. The oxygen element coexists in the oxide layer coating on LM particles and TPU macromolecules. The distribution of the four elements coincides, outlining a spherical shape. Noticeably, the intensity of C element rises before the Ga/In from outside to inside (around 10 nm ahead), consistent with previous reports.[56] This indicates that TPU forms a uniform and substantial layer coating on the eGaIn particle, thus guaranteeing a good dispersion of LM particles and a strong affinity between eutectic and TPU. The surface oxidation state of the eGaIn can be directly observed from the cross-sectional EDS mapping of an eGaIn particle presented in Figure 2C. The oxygen signal is confined to an extremely thin layer, with a penetration depth of only approximately 10 nm. This observation is consistent with other literature.[57,58] Also, the strong interfacial affinity among the metal@TE leg, eutectic, macromolecules, and organic substrates concurrently ensures the adaptive deformation and robust connection between the rigid TE legs and flexible substrate.

Furthermore, to verify the superior affinity of developed OEC ink, normalized contact areas of pure eGaIn and the OEC ink on different substrates are estimated (Figure 2D; Note S2; Table S3). It can be seen that, except for certain metals (Au, Cu) that can react to form compounds, pure eGaIn shows large contact angles (around 120°, Figure S10) on the representative organic and inorganic nonmetal substrates, implying poor surface wettability and contact area for heterointerface bonding. In contrast, the ink exhibits low contact angles across organic, inorganic nonmetal, and metal substrates. The large contact area (lower contact angle) of OEC ink brings forth a higher work of adhesion, superior wettability, and universal printability on elastomeric, plastic, ceramic, and metal substrates (Figure S11), which is particularly critical for the initial printing of circuits (Figure S12). Further thermogravimetric analysis demonstrated the stability of OEC ink (Figure S13). Since both thermal and electrical properties are critical factors for heat-to-electricity and electricity-to-heat conversion,[59] further study on the thermal and electrical contact interface of the OEC electrode was conducted (Figures S14 and S15; Table S4). With 5 kPa pressure,[59] the thermal contact resistance (TCR) of 36 and 50 μm inactivated OEC inks were 88 and 236 $mm^2\ K\ W^{-1}$, while the TCR of activated inks were decreased to 64 and 72 $mm^2\ K\ W^{-1}$, respectively. As shown in Table S5, the TCR of the OEC electrode in this work was close to that of carbon-based thermal interface material. The contact resistance at the interface between the OEC electrode and the TE legs was further evaluated using the transfer line method (TLM, Figure S15). The measured values of 2.2–2.9 mΩ are comparable with that of soldering on the Cu electrode with tin,[21] indicating that the OEC electrode is suited to large-scale TE devices with low resistance.

Electromechanical and robustness characterization of the OEC interconnects

Benefiting from the freely deformable property, the hyperbolic OEC structure could improve the robustness of the interface electrical connection. As a common scenario, ever-deforming skin will be apt to deformation differences across heterointerfaces due to modulus mismatch (e.g., lifting the TE legs off from the substrate), which is one of the main failure factors in wearable TE devices. Unlike traditional tin-based soldering with rigid connection, such mutual wetting structure ensures TE legs are capable of being shifted out of the plane with a stable circuit connection, as shown in Figures 3A and S16. Owing to the high electrical conductivity and fluid nature of the eutectic layer, the electrical connection remains highly stable (with resistance change less than 0.5%) until pulled up to 2.7 mm. It is obvious that the connection of the circuit can be restored with the re-contact of the OEC, which will be discussed later. Meanwhile, similar tests were conducted in aqueous solutions of PU (Figure 3A) to verify the connection stability in the packaging process, showing a stable electrical connection as well. Remarkably, the resistance only has negligible variation before fracture in both air and aqueous solution, indicating that the high surface energy of LM can effectively prevent the solution from penetrating the interface to break the current path. Moreover, similar stable electrical connection behaviors were demonstrated when displacements occurred in the horizontal direction. In addition to the vertical and a certain horizontal direction, the resistance remains constant even when the relative displacement between the electrode and TE leg occurs omnidirectionally (Figures 3B and S17). As shown in Figure 3B, the TE leg moves 0.5 and 1 mm away from its initial position (25% and 50% of LM electrode width, respectively) successively in 12 directions, and the resistance remains stable throughout because of the stable electrical connection. Notably, even if the displacement is performed in the PU aqueous solution (Figure S17), the resistance remains highly stable. These results are pivotal for the simplification of device fabrication with dense integration of TE legs for power density multiplication. Additionally, sheet resistance measurements of the electrode indicate that the electrical conductivity of its active layer is approximately $2.83 \times 10^6\ S\ m^{-1}$, which is close to that of pure LM ($3.4 \times 10^6\ S\ m^{-1}$).[60] Besides the electrical interconnection, an adequate mechanical anchoring force between the TE legs and substrates is necessary in device integration. Thus, the adhesive force of OEC in multi-direction was tested, where more than 5 mN is shown alongside a large displacement relative to the dimension of a single TE leg (Figures 3C, S18, and S19). Furthermore, we conducted resistance change tests on the OEC connections under different states (stretching, bending, and bending cycles), and the results demonstrated the excellent stability of our OEC (Figure S20). Also, the fluid-like nature of LM layer is not only beneficial to the connection between TE legs and flexible substrate but also offers self-healing capability (Figure 3D). When the LM-printed PU substrate is cut or broken,

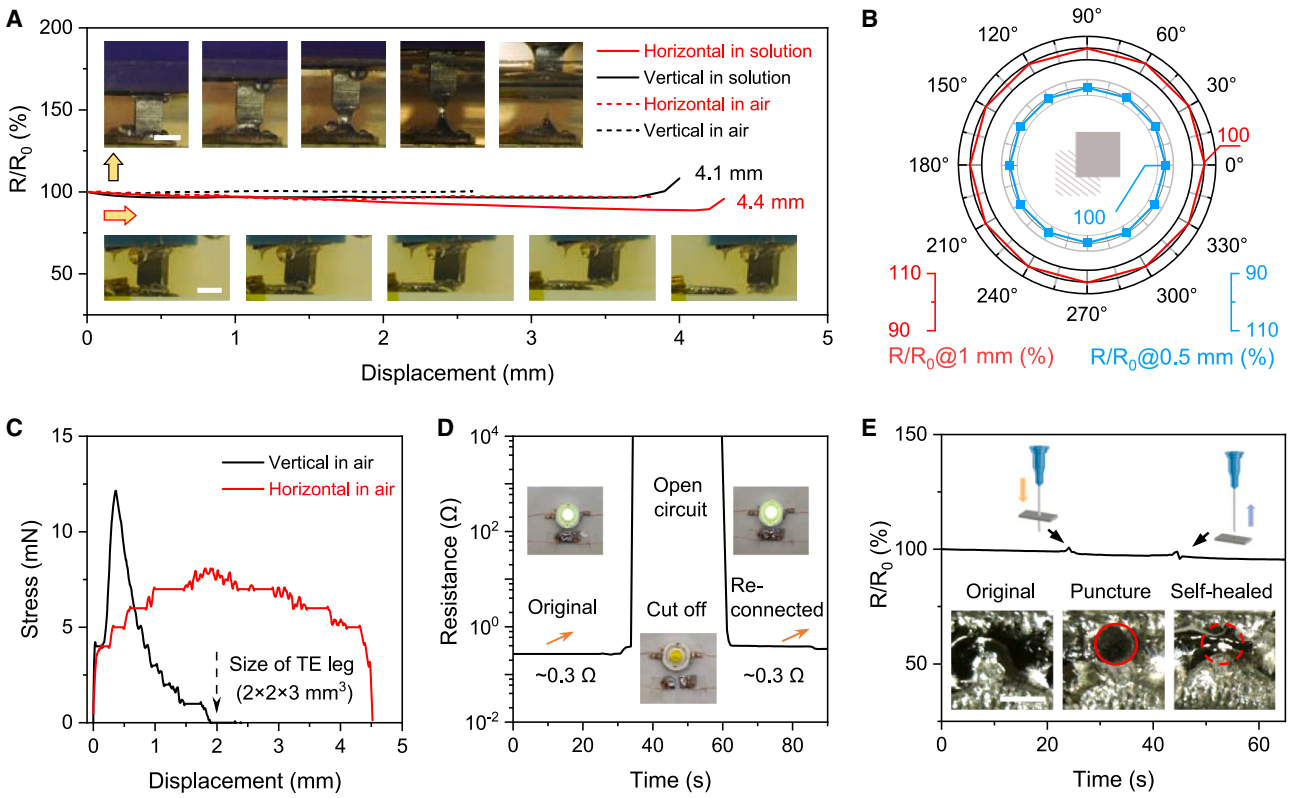

Figure 3. Electromechanical and robustness characterization of OEC interconnects

(A) Relative electrical resistance changes of the OEC interconnects during vertical/horizontal displacement in air and in PU solution. Insets, optical images of OEC interconnects at different vertical (upper row) and horizontal (lower row) displacements. Scale bars: 2 mm.

(B) Relative electrical resistance changes of OEC interconnects in different in-plane displacements in air. The red and blue lines represent a fixed displacement of 1 and 0.5 mm, respectively.

(C) The stress-displacement curves of OEC interconnects during vertical/horizontal displacement.

(D) Electrical resistance change of OEC interconnect after cut and reconnected. Insets, instant healing of an OEC interconnect used to light up an LED circuit.

(E) Electrical resistance change of OEC interconnects during the puncturing test. The top insets schematize the puncture process, and the bottom insets are the optical microscopical images of the OEC at the puncture location. Scale bars: 1 mm.

the LED turns off (bottom middle). Bringing the interfaces back to contact leads to immediate healing of the electrical conductivity, and the LED turns on again (right). The resistance of the electrode under puncture is also demonstrated in Figure 3E, where the insertion and removal of the needle produce only a small fluctuation in the resistance of the electrode, enabling it to self-heal defects in the device even after the device is packaged.

Electromechanical modeling and characterization of the TE device

In terms of the device implementation for wearable heat harvesting and cooling, an optimizable geometry with mechanical robustness and large temperature gradient is required to be configured. According to the finite element modeling (Figures 4A–4C, S21, and S22), under a reasonable load pressure for bendable scenarios (see methods), the relative displacement, output power density, and volumetric flexibility of the TE device (Figures 4D and 4E) could be varied substantially with respect to the area fill factor, i.e., the modulated air gap between adjacent TE legs. Given the facts that the reduced air gap (a larger fill factor, Figure S21) between adjacent TE legs could contribute to power density multiplication (a lower electrical resistance and large heat conduction[25,26]) while against displacement for volumetric strain propagation or redistribution across the TE device (Figures 4C and 4D), the relative displacement is a function of area fill factor, and the inset (Figure 4D) presents displacement difference between top and bottom layers of the TE device (Figures 4C and S22) and corresponding position at a fixed area fill factor of 31% (marked as red scatter). We also supplemented the modeling profile of strain distribution across the TE module in the *xyz*, *yz*, and *xz* planes (Figure S22), respectively. These results confirm the displacement for both compression and stretching. Consequently, an area fill factor of ~31% was selected to configure the TE device with a compromise between power density maximization and good flexibility. To further improve the capacity for effective heat harvesting and cooling with dense TE pairs, potential challenges such as thermal management/resistance of each layer from the substrate to TE legs, the uniform printability at large-scale, and the adhesion robustness require further investigation in the future.

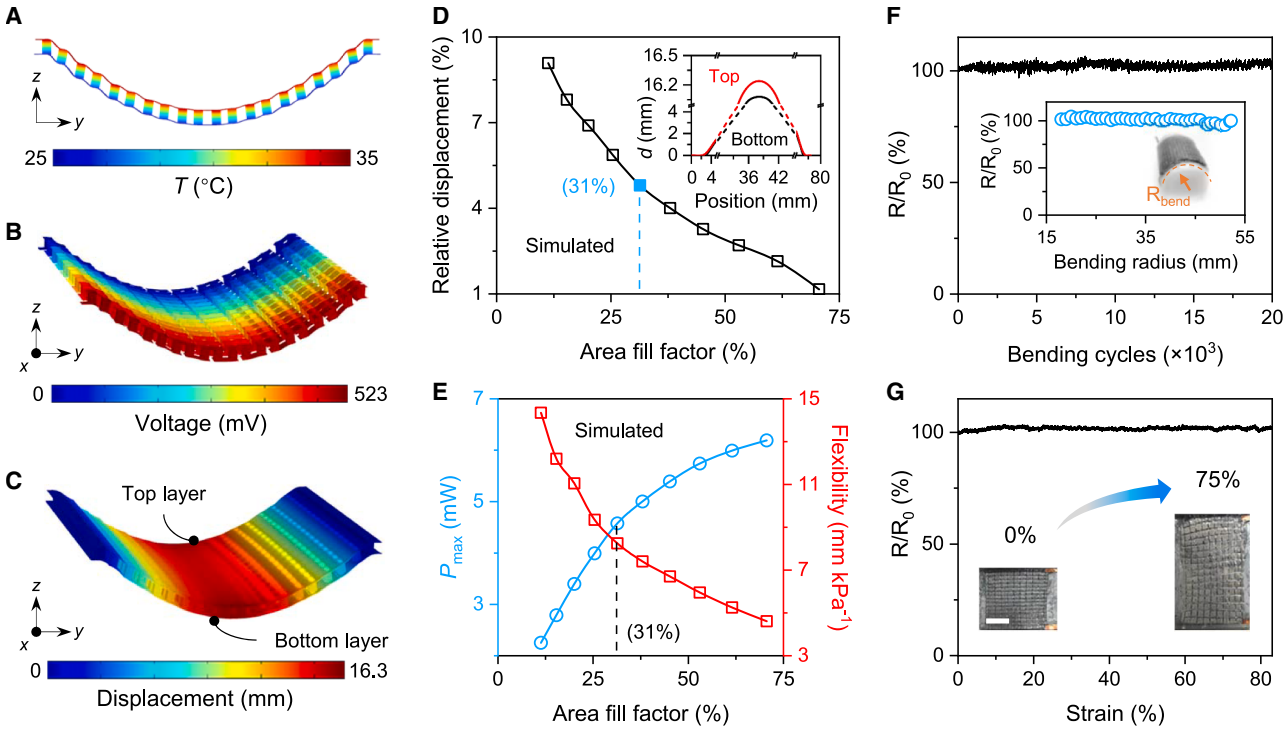

Figure 4. Electromechanical modeling and characterization of the TE device

(A–C) (A) Modeling results of cross-sectional temperature distribution, (B) voltage profile, and (C) displacement profile of the TE device at a given temperature gradient of 10°C and applied pressure of 2 kPa. Details can be seen in methods.

(D) Relative displacement as a function of area fill factor. Inset, displacement difference between top and bottom layers of the TE device extracted from the modeling profile of (C) and corresponding position at a fixed area fill factor of 31% (marked as red scatter).

(E) Modeling results of power generation and flexibility versus area fill factor.

(F) Relative resistance variation of the TE device during 20,000 bending cycles with a bending radius of 30 mm. Insets, internal resistance of the TE device under different bending radii.

(G) Relative resistance variations of the TE device versus different tensile strains. Insets, photos of the device in different stretchable states. Scale bars: 2 cm.

Then, the TE device with 160 pairs of TE legs on a TPU substrate was successfully fabricated (see methods and Figure S23). Considering the visual aesthetics, reliability, and user comfort for TE devices to be fully wearable, a high mechanical robustness, flexibility, and bendability while maintaining device performance are crucial criteria. As a consequence, the flexibility of the TE device was characterized (Figure 4E). The negligible fluctuation of internal resistance (of <4.5% under a bending radius of 52 to 18 mm) demonstrates exceptional electromechanical robustness, and there is no deterioration in electrical connection for bending radius below 18 mm. Aside from that, the TE device was subjected to a cyclic bending test under a radius of 30 mm for more than 20,000 cycles (Figure 4F) to validate the electromechanical fatigue and durability of our developed OEC interconnects. The resistance merely increases by 1.6% after 20,000 cycles of bending, suggesting excellent reliability and durability. The enlarged side views of the TE device under bending and stretching are shown in Figure S24, where the n- and p-type legs remain stable connections to the substrate within the deformable TE device. Moreover, we applied a variety of mechanical stresses to the device to validate its wearability. The device exhibited stable electromechanical behavior and strain-insensitive performance with a negligible resistance change ($\Delta R/R_0$ of 2.32% at 83% strain) until the device fell off the fixture (Figure 4G). It is worth noting that the resistance of the device remained consistent during three repetitive tests, which indicates the excellent robustness of the TE device and its stretch-proof ability (Figure S25). Furthermore, the environmental robustness of the TE device was verified by exposing it to a range of complex conditions/scenarios, simulating natural environments such as hot weather, high humidity, exposure to sweat, and alternating high-low temperatures (Figure S26). The negligible variation in electrical resistance recorded under these harsh conditions validates excellent durability and reliability of the TE device.

Power generation and active cooling performance of the TE device

The power and voltage output of the f-TEG under various temperature differences were estimated to evaluate heat harvesting and cooling performance (Figure 5). The device generates a high open-circuit voltage (V_{oc}) of 520 mV and a maximum output power (P_{max}) of 4.56 mW at an apparent temperature difference (ΔT) of ~10°C (Figure 5A). Moreover, the normalized power density (i.e., the average power generation ability by normalizing the

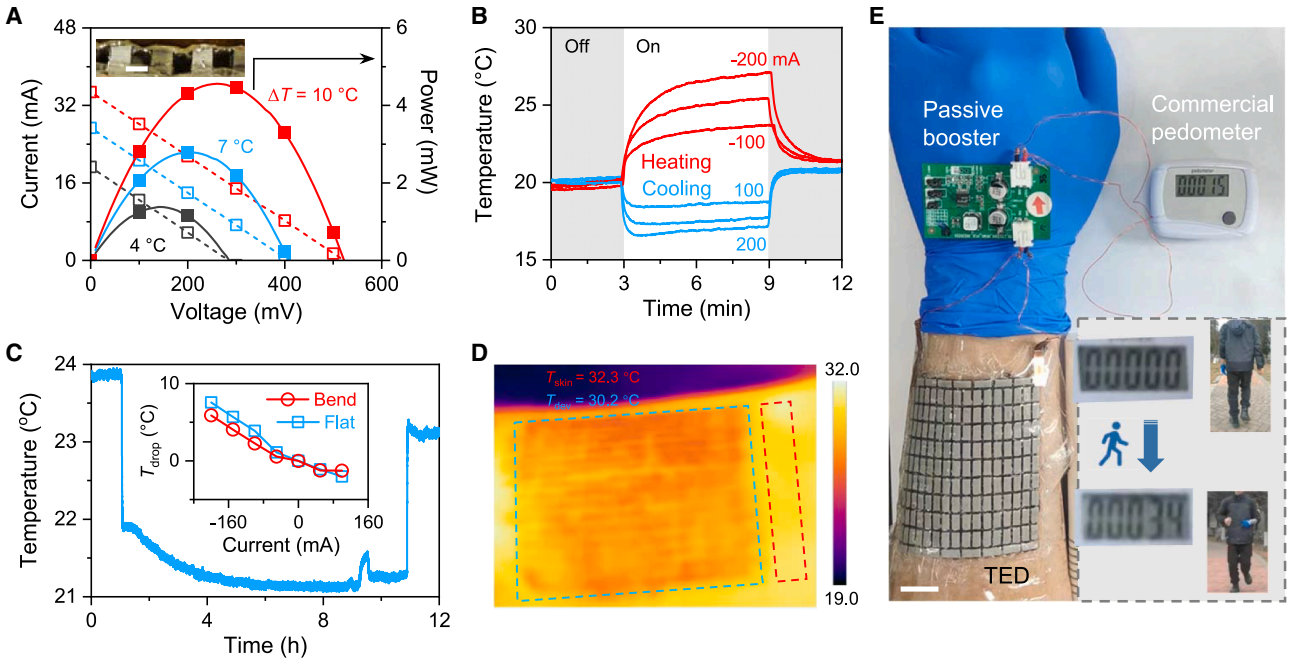

Figure 5. Heat harvesting and cooling performance of the flexible TE device

(A) Power generation of the TE device under different temperature differences. Inset, side view of the TE device at a room temperature of 16.3°C. Scale bars: 2 mm.

(B) Real-time surface temperature curves of the TE device under different input currents without a heat sink.

(C) Long-time (10 h) cooling test of the TE device at an applied current of 100 mA. Inset, current-dependent temperature changes at flat and bent states.

(D) IR image of the skin cooled by the TE device.

(E) Optical image of the TE device continually powering a commercial pedometer by entirely relying on body heat. Inset, the pedometer reading increases from 0 to 34 after jogging. Scale bars: 1 cm.

dependency of ΔT^2) was obtained to be 1.178 μW cm^{-2} K^{-2} (calculated from the ratio between the measured maximum power density and corresponding square temperature gradient across the TE device). This value is competitive compared with recently reported flexible TE generators and can be increased further with a large area fill factor, as summarized in Figure 1E and Table S2. The inset in Figure 5A presents the side view of the TE device, where the TE legs were fixed and separated by air gaps. Benefiting from the low electrical and thermal contact resistance of the OEC electrode (Figures S14 and S15), the device can achieve active thermal regulation without a heat sink. Under an input electric current of 200 mA, a maximum temperature drop (ΔT_{cool}) of 3.4°C was achieved, and the cooling effect of the device can be further enhanced with a heat spreader (Figure 5B). Figure 5C plots the long-time cooling ability of the device at flat and bent states (presented in the inset). In the long-term cooling test, the temperature immediately dropped by ~2.1°C and was maintained for 9 h under an applied current of 100 mA. The slight discrepancy in device performance (e.g., output power or voltage) between the flat and bent states stems from a difference in thermal boundary conditions during testing. The cooling effect of the device at different currents from 100 to −200 mA in the bent state showed negligible reduction compared with the flat state, implying good stability when applied to irregular surfaces like human skin. To practically validate the on-body cooling effect, the TE device was wrapped around the human upper arm. As seen in the infrared (IR) image of the arm in Figure 5D, the skin surface was successfully cooled down by an average of 2°C despite the continuous metabolic heat. This discrepancy primarily originates from the substantial metabolic heat generation of the human body and evaporative cooling through bodily fluids such as sweat. In wearable TE devices, the interface formed between the organic substrate and the skin surface impedes the natural evaporation of perspiration, thereby diminishing the overall heat dissipation capacity and ultimately compromising the cooling efficacy. It should be noted that the cooling performance of the TE device can be further improved by improving the thermal conductivity of the substrates as well as introducing an extra heat sink. With the electricity generated from the thermal gradient between human skin and the ambient, the device is capable of self-powering commercial electronic products through a passive booster, and Figure S27 presents the power generation performance of the device when it was attached to the human arm at different ambient temperatures. The temperature difference across the two surfaces of the device generated a maximum V_{oc} of 45.6 mV and a P_{max} of 40 μW at an ambient temperature of 16°C. To further evaluate the energy-harvesting capability of the device on the human body, we placed the device on the elbow and collected voltage output under both static and dynamic (motion) conditions, with the results presented in Figure S28. When the human arm bends, the conformal contact

between the device and the skin is enhanced, leading to an increase in output voltage. When the arm straightens, the output voltage drops back to the level observed in the static state. This indicates that the device possesses excellent deformability to conform to human body movements. The effect of motion-induced skin heat exchange on the overall output performance is more significant than that caused by resistance variation. When a passive voltage booster was adopted to boost the produced voltage (the photo and circuit diagram of the passive booster are shown in Figure S29), the V_{oc} can be increased to 2.35, 3.30, 4.10, and 5.00 V accordingly. Thus, the device can sustain various commercial wearable devices with on-demand voltage supplies. For example, 3.3 V was achieved to continuously power a commercial pedometer when the TE device was worn on the arm (Figures 5E and S30), in the absence of a battery. Also, the device was practically tested to determine its performance during exercise, as shown in Video S1, where the device serves as a wearable power source to power the commercial pedometer to count steps. Our device can stably use body heat to power a commercial pedometer with a stable package on the human forearm across different scenarios. Meanwhile, blue and white LED lights can also be stably driven even at higher room temperatures (22.6°C), as shown in Figure S31. This indicates that our device can supply a sustained and sufficient power supply for various commercial wearable electronic devices.

Conclusion

We developed a deformable OEC interconnect to advance wearable TE devices with superior flexibility, stretchability, and robustness. The OEC interconnects patterned on the organic substrate promoted self-organization of amphiphilic bilayer structures, facilitating stable electrothermal conduction with rigid inorganic TE legs under combined deformation. Moreover, the strong affinity and deformability endowed the TE device with a robust electromechanical connection against multi-axial bending and displacement. The wearable TE device, consisting of 160 pairs of TE legs, demonstrates outstanding prototype-level stretchability, flexibility, and robustness, which successfully achieve both body cooling and power generation functions. With a passive booster, the as-fabricated TE device continuously powers various consumer electronics successfully by entirely using waste body heat. This state-of-the-art heterointerface bonding through deformable interconnects offers a universal strategy to bridge flexible organic substrates and rigid inorganic components, which can be promisingly used in a variety of wearable devices.

METHODS

Materials

$Bi_{0.4}Sb_{1.6}Te_3$ and $Bi_2Te_{2.85}Se_{0.15}$ commercial materials (Shenzhen Thermo-Electric New Energy Technology Co., Ltd) were used for p- and n-type TE legs, respectively. EGaIn alloy (75.5% Ga, 24.5% In) was purchased from Huantai Metal Material Co., Ltd (Dongguan, China). TPU organic substrates were purchased from Shuntai Plastic (Shenzhen, China). PU aqueous solution and TPU particle (Lubrizol Pearlstick 5703) were purchased from Jitian Chemical Co., Ltd (Shenzhen, China).

Preparation of OEC ink

Firstly, 1 g eGaIn LM and 1 mL cyclohexanone were added into 2 mL tubes and then sonicated at a power output of 130 W for 2 min with a probe sonicator (Sonics Vibra-Cell VCX130, 2 s on and 3 s off cycling). The suspension was then centrifuged for 2 min at 4,500 rpm, and the supernatant was removed. Secondly, 0.4 g pp-TPU particle was added to the 2 g cyclohexanone, and the mixture was heated and stirred for 3 h at 50°C until all the TPU particles were dissolved. Finally, 0.125 g as-prepared TPU solution was mixed with the above eGain suspension and stirred to form a uniform OEC ink. The ink was then dried in an oven at 70°C for ~30 min to remove excess solvent and achieve a suitable viscosity for stencil printing.

Patterned printing of OEC ink on TPU substrates

Prior to printing, the TPU substrates were covered by customized masks. The OEC ink was then printed onto substrates via a stencil printing process with the aid of a blade, and the printed traces were then placed in the oven at 70°C for 15 min to thoroughly dry. To activate the traces, an eGaIn-infiltrated foam (polystyrene foam with a small amount of eGaIn coated on its surface) with a small amount of LM coated on its surface was pressed onto the traces and pulled forward to activate the eGaIn particles by the shearing and pressure force. Finally, the traces were turned into a shiny silver color, and the masks were removed to obtain the OEC pattern.

Finite element modeling

Finite element analysis (FEA) was employed by using COMSOL Multiphysics (coupled with heat transfer in solids, electric currents, solid mechanics, and electrical circuit modules) to facilitate geometry-dependent electro-thermo-mechanical optimization for the TE device. The thermoelectric effect, electromagnetic heating, and thermal expansion were included in Multiphysics, and detailed flowcharts and component definitions can be found in our previous work.[21] The measured electromechanical and thermal properties of OEC in this work and TE materials previously reported were utilized in the simulation. The hot- and cold-side temperatures were fixed at 35°C and 25°C, respectively, according to the experimental thermal measurement. The width (w_te) and length (l_te) of the TE device were invariable from the experiment. In the modeling, the width (w_leg) of TE legs and the gap (g_leg) between adjacent TE legs (Figure S21) were parametrically swept to change the areal fill factor at a known volumetric pressure. The maximal output power was estimated by using 0.25 times the open-circuit voltage and the short-circuit current.

Fabrication of the flexible TE device

First, the TPU substrate with patterned OEC ink was placed on a horizontal porous substrate (porous alumina plate) as the bottom electrode. Then n- and p-type TE legs sputtered by Au nanoparticles were placed alternatively on the OEC patterns. The TE legs have a cross-section area of 2 mm × 2 mm and a height of 3 mm, and the details of placement are diagrammed in Figure S23. Afterward, the top electrodes were aligned with the n- and p-type TE legs array and vertically mounted on accordingly. Then, PU aqueous solution is injected into the sandwiching gap between the PU substrates to immerse the

TE legs and left in the oven at 80°C for 6 h to ensure that the water solution fully dries up. After drying, a thin but robust PU film will encapsulate the TE legs and PU electrodes to realize device integration. The resistance of the TE device is ~15 Ω (Figure 5A), with an overall active area of 68 mm × 60 mm.

Characterizations of OEC interconnects and TE devices

The microstructure and elemental composition were characterized by transmission electron microscopy (TEM, Tecnai G2 F20 S-Twin TMP). The EDS mapping of the sample was completed on SEM (Zeiss GeminiSEM 300; Thermo Scientific Apreo 2S and Oxford Ultim Max) and EDS. The contact angle of eGaIn and OEC ink on various substrates was characterized using an optical microscope (GP-660V). IR images were captured by an IR camera (FLIR A300-series). The power generation of the flexible TE device was tested by a homemade temperature controller, where the bottom surface was attached to a semiconductor chilling plate to maintain a constant temperature and different temperatures were applied on the top surface by another semiconductor chilling plate. The temperature difference of the device is obtained by measuring the top and bottom substrates through an IR camera. The V_{OC}, as well as output power, was tested via a Keithley 2400 source meter. The resistance was tested via a Keithley 2182 source meter instrument by sweeping the voltage from −1 to +1 V with a step size of 0.01 V and obtaining the resistance value through linear fitting of the resulting I-V curve. The real-time temperature of the device during cooling or heating was monitored by a K-type thermocouple (UNIT-UT325). To investigate the element distribution in different regions in the OEC electrode, a smooth silicon slice with a sputtered Au layer was closely attached to a polyethylene terephthalate (PET) substrate with activated OEC ink at room temperature for 1 h and then separated from the middle. The inevitable shear forces during separation induce the formation of a continuous LM layer on the separated interface. Then, silicon and PET substrates are stripped by tape repeatedly to remove the ink till the surface is uniform, subsequently characterized by SEM-EDS. The thermal contact resistance of LM particle ink was tested in a vacuum environment with a homemade test device as shown in Figure S14. Two brass blocks with known thermal diffusion coefficients and the sample to be measured are stacked up to form a sandwich structure. Then, its top side is connected to a heater while 4 thermocouples are used to record the temperatures of the top and bottom interfaces of each brass block. The contact resistance was measured via the transfer line model using a Keithley 2182 nanovoltmeter for the electrical measurements. Detailed calculation process of the contact resistance of the samples was presented in Figure S15. The stretchability, flexibility, and cycling stability of the device were characterized by a universal tensile tester (Shimadzu AG-X), and the resistance was measured simultaneously by a multimeter (Keithley DMM6500).

RESOURCE AVAILABILITY

Lead contact

Further information and requests for resources and materials should be directed to and will be fulfilled by the lead contact, Tianpeng Ding (dingtp@uestc.edu.cn.).

Materials availability

This study did not generate new unique reagents.

Data and code availability

The datasets generated during and/or analyzed during the current study are available from the corresponding author on reasonable request. The code utilized during the current study is available from the corresponding author on reasonable request.

ACKNOWLEDGMENTS

This research was supported by the National Key Research and Development Program of China (grant no. 2024YFA1210400 [J.H.]), the National Natural Science Foundation of China (grant nos. 52472088 [T.D.], 52202084 [T.D.], 12434001 [J.H.], 52461160258 [J.H.], 52422205 [X.X.], 52403154 [W.X.]), the Outstanding Scholarship Foundation of UESTC (grant no. A1098531023601345 [T.D.]), the Natural Science Foundation of Sichuan Province (grant no. 2023NSFSC0959 [T.D.]), the Guangdong Provincial Key Laboratory of Advanced Thermoelectric Materials and Device Physics (grant no. 2024B1212010001 [J.H.]), the Outstanding Talents Training Fund in Shenzhen (grant no. 202108 [J.H.]), the Ministry of Education of Singapore (grant no. A-8002978-00-00 [G.W.H]), NUS research support (A-8003994-00-00 [G.W.H.]), and the China Postdoctoral Science Foundation (grant no. 2025M770159 [W.X.]). Y.Z. acknowledges support from the Advanced Research and Technology Innovation Centre (ARTIC), the National University of Singapore (Project No. AFP-RP3) and ARTIC Fellowship (grant no. A-8003964-00-00). The authors appreciate Dr. Tingchuan Zhou from Analysis and Testing Center, University of Electronic Science and Technology of China, for technical support.

AUTHOR CONTRIBUTIONS

Z.D., T.D., and W.X. conceived the idea and designed the experiments. T.D., G.W.H., J.H., and W.X. supervised the project. Z.D., Y.Z., and S.C. contributed to the device fabrication, characterization, and FEA simulation. Z.D., X.X., G.W.H., S.L., X.C., and Y.T. contributed to data measurement and analysis. Z.D., T.D., Y.Z., and W.X. contributed to the writing, and all authors revised the manuscript.

DECLARATION OF INTERESTS

The authors declare no competing interests.

SUPPLEMENTAL INFORMATION

Supplemental information can be found online at https://doi.org/10.1016/j.matt.2026.102653.

Received: August 18, 2025
Revised: November 19, 2025
Accepted: January 4, 2026
Published: March 4, 2026

REFERENCES

1. Arwani, R.T., Tan, S.C.L., Sundarapandi, A., Goh, W.P., Liu, Y., Leong, F.Y., Yang, W., Zheng, X.T., Yu, Y., Jiang, C., et al. (2024). Stretchable ionic-electronic bilayer hydrogel electronics enable in situ detection of solid-state epidermal biomarkers. Nat. Mater. *23*, 1115–1122. https://doi.org/10.1038/s41563-024-01918-9.
2. Zeng, Q., Tian, X., Nguyen, D.T., Li, C., Chia, P., Tee, B.C.K., Wu, C., and Ho, J.S. (2024). A digitally embroidered metamaterial biosensor for kinetic environments. Nat. Electron. *7*, 1025–1034. https://doi.org/10.1038/s41928-024-01263-4.

3. Ates, H.C., Yetisen, A.K., Güder, F., and Dincer, C. (2021). Wearable devices for the detection of COVID-19. Nat. Electron. *4*, 13–14. https://doi.org/10.1038/s41928-020-00533-1.

4. Sugahara, T., Ekubaru, Y., Nong, N.V., Kagami, N., Ohata, K., Hung, L.T., Okajima, M., Nambu, S., and Suganuma, K. (2019). Fabrication with Semiconductor Packaging Technologies and Characterization of a Large-Scale Flexible Thermoelectric Module. Adv. Mater. Technol. *4*, 1800556. https://doi.org/10.1002/admt.201800556.

5. Zhang, Y., Ge, B., Feng, J., Kuang, N., Ye, H., Yuan, Z., Wu, M., Jiang, B., Li, J., Sun, Q., et al. (2024). High-Performance Self-Powered Flexible Thermoelectric Device for Accelerated Wound Healing. Adv. Funct. Mater. *34*, 2403990. https://doi.org/10.1002/adfm.202403990.

6. Zhu, P., Du, H., Hou, X., Lu, P., Wang, L., Huang, J., Bai, N., Wu, Z., Fang, N.X., and Guo, C.F. (2021). Skin-electrode iontronic interface for mechanosensing. Nat. Commun. *12*, 4731. https://doi.org/10.1038/s41467-021-24946-4.

7. Cheng, Y., Zhou, Y., Wang, R., Chan, K.H., Liu, Y., Ding, T., Wang, X.-Q., Li, T., and Ho, G.W. (2022). An Elastic and Damage-Tolerant Dry Epidermal Patch with Robust Skin Adhesion for Bioelectronic Interfacing. ACS Nano *16*, 18608–18620. https://doi.org/10.1021/acsnano.2c07097.

8. Cao, Y., Tan, Y.J., Li, S., Lee, W.W., Guo, H., Cai, Y., Wang, C., and Tee, B.C.K. (2019). Self-healing electronic skins for aquatic environments. Nat. Electron. *2*, 75–82. https://doi.org/10.1038/s41928-019-0206-5.

9. Ding, T., Chan, K.H., Zhou, Y., Wang, X.-Q., Cheng, Y., Li, T., and Ho, G.W. (2020). Scalable thermoelectric fibers for multifunctional textile-electronics. Nat. Commun. *11*, 6006. https://doi.org/10.1038/s41467-020-19867-7.

10. Hong, S., Gu, Y., Seo, J.K., Wang, J., Liu, P., Meng, Y.S., Xu, S., and Chen, R. (2019). Wearable thermoelectrics for personalized thermoregulation. Sci. Adv. *5*, eaaw0536. https://doi.org/10.1126/sciadv.aaw0536.

11. Osborn, L.E., Venkatasubramanian, R., Himmtann, M., Moran, C.W., Pierce, J.M., Gajendiran, P., Wormley, J.M., Ung, R.J., Nguyen, H.H., Crego, A.C.G., et al. (2024). Evoking natural thermal perceptions using a thin-film thermoelectric device with high cooling power density and speed. Nat. Biomed. Eng. *8*, 1004–1017. https://doi.org/10.1038/s41551-023-01070-w.

12. Miao, L., Zhu, S., Liu, C., Gao, J., Zhang, Z., Peng, Y., Chen, J.-L., Gao, Y., Liang, J., and Mori, T. (2024). Comfortable wearable thermoelectric generator with high output power. Nat. Commun. *15*, 8516. https://doi.org/10.1038/s41467-024-52841-1.

13. Kishore, R.A., Nozariasbmarz, A., Poudel, B., Sanghadasa, M., and Priya, S. (2019). Ultra-high performance wearable thermoelectric coolers with less materials. Nat. Commun. *10*, 1765. https://doi.org/10.1038/s41467-019-09707-8.

14. Nozariasbmarz, A., Collins, H., Dsouza, K., Polash, M.H., Hosseini, M., Hyland, M., Liu, J., Malhotra, A., Ortiz, F.M., Mohaddes, F., et al. (2020). Review of wearable thermoelectric energy harvesting: From body temperature to electronic systems. Appl. Energy *258*, 114069. https://doi.org/10.1016/j.apenergy.2019.114069.

15. Xu, Q., Deng, B., Zhang, L., Lin, S., Han, Z., Zhou, Q., Li, J., Zhu, Y., Jiang, F., Li, Q., et al. (2022). High-performance, flexible thermoelectric generator based on bulk materials. Cell Rep. Phys. Sci. *3*, 100780. https://doi.org/10.1016/j.xcrp.2022.100780.

16. Zhu, P., Shi, C., Wang, Y., Wang, Y., Yu, Y., Wang, Y., Deng, Y., and Xiao, J. (2021). Recyclable, Healable, and Stretchable High-Power Thermoelectric Generator. Adv. Energy Mater. *11*, 2100920. https://doi.org/10.1002/aenm.202100920.

17. Hao, X., Wang, J., and Wang, H. (2025). High power output density organic thermoelectric devices for practical applications in waste heat harvesting. Chem. Soc. Rev. *54*, 1957–1985. https://doi.org/10.1039/D4CS01045K.

18. Wang, D., Ding, J., Ma, Y., Xu, C., Li, Z., Zhang, X., Zhao, Y., Zhao, Y., Di, Y., Liu, L., et al. (2024). Multi-heterojunctioned plastics with high thermoelectric figure of merit. Nature *632*, 528–535. https://doi.org/10.1038/s41586-024-07724-2.

19. Zhou, Y., Ding, T., Cheng, Y., Huang, Y., Wang, W., Yang, J., Xie, L., Ho, G.W., and He, J. (2023). Non-planar dielectrics derived thermal and electrostatic field inhomogeneity for boosted weather-adaptive energy harvesting. Natl. Sci. Rev. *10*, nwad186. https://doi.org/10.1093/nsr/nwad186.

20. Zhou, Y., Guo, Z., and He, J. (2020). Redesign high-performance flexible thermoelectrics: From mathematical algorithm to artificial cracks. Appl. Phys. Lett. *116*, 043904. https://doi.org/10.1063/1.5132827.

21. Zhou, Y., Liu, X., Jia, B., Ding, T., Mao, D., Wang, T., Ho, G.W., and He, J. (2023). Physics-guided co-designing flexible thermoelectrics with techno-economic sustainability for low-grade heat harvesting. Sci. Adv. *9*, eadf5701. https://doi.org/10.1126/sciadv.adf5701.

22. Hyland, M., Hunter, H., Liu, J., Veety, E., and Vashaee, D. (2016). Wearable thermoelectric generators for human body heat harvesting. Appl. Energy *182*, 518–524. https://doi.org/10.1016/j.apenergy.2016.08.150.

23. Suarez, F., Parekh, D.P., Ladd, C., Vashaee, D., Dickey, M.D., and Öztürk, M.C. (2017). Flexible thermoelectric generator using bulk legs and liquid metal interconnects for wearable electronics. Appl. Energy *202*, 736–745. https://doi.org/10.1016/j.apenergy.2017.05.181.

24. Yang, Q., Yang, S., Qiu, P., Peng, L., Wei, T.-R., Zhang, Z., Shi, X., and Chen, L. (2022). Flexible thermoelectrics based on ductile semiconductors. Science *377*, 854–858. https://doi.org/10.1126/science.abq0682.

25. Wang, Y., Li, A., Hong, Y., Deng, T., Deng, P., Huang, Y., Liu, K., Wang, J., Fu, C., and Zhu, T. (2025). Iterative sublattice amorphization facilitates exceptional processability in inorganic semiconductors. Nat. Mater. *24*, 1545–1553. https://doi.org/10.1038/s41563-024-02112-7.

26. Lee, B., Cho, H., Park, K.T., Kim, J.S., Park, M., Kim, H., Hong, Y., and Chung, S. (2020). High-performance compliant thermoelectric generators with magnetically self-assembled soft heat conductors for self-powered wearable electronics. Nat. Commun. *11*, 5948. https://doi.org/10.1038/s41467-020-19756-z.

27. Sun, T., Zhou, B., Zheng, Q., Wang, L., Jiang, W., and Snyder, G.J. (2020). Stretchable fabric generates electric power from woven thermoelectric fibers. Nat. Commun. *11*, 572. https://doi.org/10.1038/s41467-020-14399-6.

28. Ochirkhuyag, N., Matsuda, R., Song, Z., Nakamura, F., Endo, T., and Ota, H. (2021). Liquid metal-based nanocomposite materials: fabrication technology and applications. Nanoscale *13*, 2113–2135. https://doi.org/10.1039/D0NR07479A.

29. Liu, S., Shah, D.S., and Kramer-Bottiglio, R. (2021). Highly stretchable multilayer electronic circuits using biphasic gallium-indium. Nat. Mater. *20*, 851–858. https://doi.org/10.1038/s41563-021-00921-8.

30. Boley, J.W., White, E.L., Chiu, G.T.C., and Kramer, R.K. (2014). Direct Writing of Gallium-Indium Alloy for Stretchable Electronics. Adv. Funct. Mater. *24*, 3501–3507. https://doi.org/10.1002/adfm.201303220.

31. Yu, L., Feng, Y., S/O M Tamil Selven, D., Yao, L., Soon, R.H., Yeo, J.C., and Lim, C.T. (2019). Dual-Core Capacitive Microfiber Sensor for Smart Textile Applications. ACS Appl. Mater. Interfaces *11*, 33347–33355. https://doi.org/10.1021/acsami.9b10937.

32. Takaya, M., Matsuda, R., Inamori, G., Kamoto, U., Isoda, Y., Tachibana, D., Nakamura, F., Fuchiwaki, O., Okubo, Y., and Ota, H. (2021). Transformable Electrocardiograph Using Robust Liquid-Solid Heteroconnector. ACS Sens. *6*, 212–219. https://doi.org/10.1021/acssensors.0c02135.

33. Guo, R., Sun, X., Yuan, B., Wang, H., and Liu, J. (2019). Magnetic Liquid Metal (Fe-EGaIn) Based Multifunctional Electronics for Remote Self-Healing Materials, Degradable Electronics, and Thermal Transfer Printing. Adv. Sci. *6*, 1901478. https://doi.org/10.1002/advs.201901478.

34. Guo, R., Yao, S., Sun, X., and Liu, J. (2019). Semi-liquid metal and adhesion-selection enabled rolling and transfer (SMART) printing: A general method towards fast fabrication of flexible electronics. Sci. China Mater. *62*, 982–994. https://doi.org/10.1007/s40843-018-9400-2.

35. Lopes, P.A., Fernandes, D.F., Silva, A.F., Marques, D.G., de Almeida, A.T., Majidi, C., and Tavakoli, M. (2021). Bi-Phasic Ag-In-Ga-Embedded Elastomer Inks for Digitally Printed, Ultra-Stretchable, Multi-layer

Electronics. ACS Appl. Mater. Interfaces *13*, 14552–14561. https://doi.org/10.1021/acsami.0c22206.

36. Boley, J.W., White, E.L., and Kramer, R.K. (2015). Mechanically sintered gallium-indium nanoparticles. Adv. Mater. *27*, 2355–2360. https://doi.org/10.1002/adma.201404790.
37. Markvicka, E.J., Bartlett, M.D., Huang, X., and Majidi, C. (2018). An autonomously electrically self-healing liquid metal-elastomer composite for robust soft-matter robotics and electronics. Nat. Mater. *17*, 618–624. https://doi.org/10.1038/s41563-018-0084-7.
38. Zhu, P., Luo, X., Lin, X., Qiu, Z., Chen, R., Wang, X., Wang, Y., Deng, Y., and Mao, Y. (2023). A self-healable, recyclable, and flexible thermoelectric device for wearable energy harvesting and personal thermal management. Energy Convers. Manag. *285*, 117017. https://doi.org/10.1016/j.enconman.2023.117017.
39. Zadan, M., Malakooti, M.H., and Majidi, C. (2020). Soft and Stretchable Thermoelectric Generators Enabled by Liquid Metal Elastomer Composites. ACS Appl. Mater. Interfaces *12*, 17921–17928. https://doi.org/10.1021/acsami.9b19837.
40. Padmanabhan Ramesh, V., Sargolzaeiaval, Y., Neumann, T., Misra, V., Vashaee, D., Dickey, M.D., and Ozturk, M.C. (2021). Flexible thermoelectric generator with liquid metal interconnects and low thermal conductivity silicone filler. npj Flex. Electron. *5*, 5. https://doi.org/10.1038/s41528-021-00101-3.
41. Xu, Y., Wu, B., Guo, Y., Hou, C., Li, Y., Wang, H., and Zhang, Q. (2023). Flexible and stretchable thermoelectric devices with Ni-EGaIn liquid metal electrodes for cooling and low-grade-body heat harvesting. J. Alloys Compd. *945*, 169260. https://doi.org/10.1016/j.jallcom.2023.169260.
42. Sargolzaeiaval, Y., Padmanabhan Ramesh, V., Neumann, T.V., Misra, V., Vashaee, D., Dickey, M.D., and Öztürk, M.C. (2020). Flexible thermoelectric generators for body heat harvesting-Enhanced device performance using high thermal conductivity elastomer encapsulation on liquid metal interconnects. Appl. Energy *262*, 114370. https://doi.org/10.1016/j.apenergy.2019.114370.
43. Wang, R., Wu, M., Jiang, D., Liang, H., He, W., Sun, Y., and Qian, Z. (2023). Stretchable Thermoelectric Generators Based on Bulk Bi_2Te_3 and Liquid Metals. Adv. Electron. Mater. *9*, 2300300. https://doi.org/10.1002/aelm.202300300.
44. Kee, S., Haque, M.A., Corzo, D., Alshareef, H.N., and Baran, D. (2019). Self-Healing and Stretchable 3D-Printed Organic Thermoelectrics. Adv. Funct. Mater. *29*, 1905426. https://doi.org/10.1002/adfm.201905426.
45. Tan, M., Shi, X.L., Liu, W.D., Jiang, Y., Liu, S.Q., Cao, T., Chen, W., Li, M., Lin, T., Deng, Y., et al. (2025). Enabling ultra-flexible inorganic thin-film-based thermoelectric devices by introducing nanoscale titanium layers. Nat. Commun. *16*, 633. https://doi.org/10.1038/s41467-025-56015-5.
46. Liu, Y., Zhang, Q., Huang, A., Zhang, K., Wan, S., Chen, H., Fu, Y., Zuo, W., Wang, Y., Cao, X., et al. (2024). Fully inkjet-printed Ag_2Se flexible thermoelectric devices for sustainable power generation. Nat. Commun. *15*, 2141. https://doi.org/10.1038/s41467-024-46183-1.
47. Lin, S., Zhang, L., Zeng, W., Shi, D., Liu, S., Ding, X., Yang, B., Liu, J., Lam, K.-h., Huang, B., and Tao, X. (2022). Flexible thermoelectric generator with high Seebeck coefficients made from polymer composites and heat-sink fabrics. Commun. Mater. *3*, 44. https://doi.org/10.1038/s43246-022-00263-1.
48. Deng, T., Gao, Z., Li, Z., Qiu, P., Li, Z., Yuan, X., Ming, C., Wei, T.R., Chen, L., and Shi, X. (2024). Room-temperature exceptional plasticity in defective Bi_2Te_3-based bulk thermoelectric crystals. Science *386*, 1112–1117. https://doi.org/10.1126/science.adr8450.
49. Ren, W., Sun, Y., Zhao, D., Aili, A., Zhang, S., Shi, C., Zhang, J., Geng, H., Zhang, J., Zhang, L., et al. (2021). High-performance wearable thermoelectric generator with self-healing, recycling, and Lego-like reconfiguring capabilities. Sci. Adv. *7*, eabe0586. https://doi.org/10.1126/sciadv.abe0586.
50. Xu, S., Li, M., Dai, Y., Hong, M., Sun, Q., Lyu, W., Liu, T., Wang, Y., Zou, J., Chen, Z.G., and Dargusch, M. (2022). Realizing a 10 °C Cooling Effect in a Flexible Thermoelectric Cooler Using a Vortex Generator. Adv. Mater. *34*, e2204508. https://doi.org/10.1002/adma.202204508.
51. Lee, J., Sul, H., Lee, W., Pyun, K.R., Ha, I., Kim, D., Park, H., Eom, H., Yoon, Y., Jung, J., et al. (2020). Stretchable Skin-Like Cooling/Heating Device for Reconstruction of Artificial Thermal Sensation in Virtual Reality. Adv. Funct. Mater. *30*, 1909171. https://doi.org/10.1002/adfm.201909171.
52. Wei, H., Zhang, J., Han, Y., and Xu, D. (2022). Soft-covered wearable thermoelectric device for body heat harvesting and on-skin cooling. Appl. Energy *326*, 119941. https://doi.org/10.1016/j.apenergy.2022.119941.
53. Malik, Y.T., Akbar, Z.A., Seo, J.Y., Cho, S., Jang, S.Y., and Jeon, J.W. (2021). Self-Healable Organic-Inorganic Hybrid Thermoelectric Materials with Excellent Ionic Thermoelectric Properties. Adv. Energy Mater. *12*, 2103070. https://doi.org/10.1002/aenm.202103070.
54. Yang, S., Li, Y., Deng, L., Tian, S., Yao, Y., Yang, F., Feng, C., Dai, J., Wang, P., and Gao, M. (2023). Flexible thermoelectric generator and energy management electronics powered by body heat. Microsyst. Nanoeng. *9*, 106. https://doi.org/10.1038/s41378-023-00583-3.
55. Jung, S.-J., Shin, J., Lim, S.-S., Kwon, B., Baek, S.-H., Kim, S.K., Park, H.-H., and Kim, J.-S. (2021). Porous organic filler for high efficiency of flexible thermoelectric generator. Nano Energy *81*, 105604. https://doi.org/10.1016/j.nanoen.2020.105604.
56. Chen, S., Fan, S., Qi, J., Xiong, Z., Qiao, Z., Wu, Z., Yeo, J.C., and Lim, C.T. (2023). Ultrahigh Strain-Insensitive Integrated Hybrid Electronics Using Highly Stretchable Bilayer Liquid Metal Based Conductor. Adv. Mater. *35*, 2208569. https://doi.org/10.1002/adma.202208569.
57. Regan, M.J., Tostmann, H., Pershan, P.S., Magnussen, O.M., DiMasi, E., Ocko, B.M., and Deutsch, M. (1997). X-ray study of the oxidation of liquid-gallium surfaces. Phys. Rev. B *55*, 10786–10790. https://doi.org/10.1103/PhysRevB.55.10786.
58. Zavabeti, A., Ou, J.Z., Carey, B.J., Syed, N., Orrell-Trigg, R., Mayes, E.L.H., Xu, C., Kavehei, O., O'Mullane, A.P., Kaner, R.B., et al. (2017). A liquid metal reaction environment for the room-temperature synthesis of atomically thin metal oxides. Science *358*, 332–335. https://doi.org/10.1126/science.aao4249.
59. Kuang, H., Wu, B., Wang, J., Fu, J., Feng, Y., Yu, C., Wang, Z., Zhang, J., and Ji, Y. (2022). Wettability and thermal contact resistance of thermal interface material composited by gallium-based liquid metal on copper foam. Int. J. Heat Mass Transf. *199*, 123444. https://doi.org/10.1016/j.ijheatmasstransfer.2022.123444.
60. Chiechi, R.C., Weiss, E.A., Dickey, M.D., and Whitesides, G.M. (2008). Eutectic gallium-indium (EGaIn): a moldable liquid metal for electrical characterization of self-assembled monolayers. Angew. Chem., Int. Ed. *47*, 142–144. https://doi.org/10.1002/anie.200703642.